Design and Analysis on a New Underwater Robot

Ngoc-Huy Tran, Hyeung-Sik Choi*, Sang-Seob Lee, and Ba-Loc Mai

Division of Mechanical and Energy Systems Engineering, Korea Maritime University, Busan, Korea

Abstract. This paper describes the analysis of the architecture, and control system of a new underwater robot named underwater disk robot (UDR), which has six degrees of freedom (DOF) motion. With such thruster positions, the vehicle has omnidirectional manoeuvrability without heading motion. Also, the motion of the streamline disk-shaped UDR hull is less affected by side disturbances because the UDR can move robustly, swiftly along any direction, and the hull reduce the drag force on its body in the horizontal motion. Heave and pitch motion simulation studies of the UDR were carried out with the computational fluid dynamics (CFD) software. required format.

Keywords: Disk robot, autonomous underwater vehicle, CFD, PID, Extended Kalman Filter.

1 Introduction

Unmanned undersea vehicles (UUV) have become a main tool in undersea surveying for scientific, military and commercial applications, posing no risks to humans [1] [2]. Despite considerable improvements in the design and performance of UUVs, scientists and engineers still faced with the difficult tasks of designing the shapes for the UUV that will yield low hydrodynamic drag and of eliminating actuators for robust or swift motion along any direction [3] [4]. One of the shapes that have been proposed is the disk shape for the UUV hull. A disk-shaped vehicle hull is least affected by side disturbances during horizontal movement [5]. However, only few disk-shaped UUVs have been developed so far. The AQUA2 built at McGill University of Canada is flat-shaped [6].

To enhance the performance of UUVs, we have developed a new six DOF UDR with a streamline disk-shaped hull and 120-degree symmetrically disposed thrusters, as shown in Fig. 1. The horizontal thrusters are redundantly deployed so that the UDR can move in any direction with equal and robust thrust forces. In this paper, some of new features of the UDR are introduced, and its performance is presented through a theoretic analysis and experiments. In addition, pure heave motion and pure pitch motion studies were conducted to emulate the vertical planar motion mechanism (VPMM) test by CFD motion analysis.

* Corrsponding author.

J. Lee et al. (Eds.): ICIRA 2013, Part II, LNAI 8103, pp. 289–301, 2013.

The paper is organized as follows: in section 2, the design of mechanical and control system is presented; in section 3, a dynamics model; and in section 4, a motion analysis of the UDR using CFD software is presented.

2 Vehicle Design

2.1 Mechanical Design

The body of the UDR is designed as disk-shaped vehicle in order to minimize the effect of water resistance from side disturbances such as currents or wave effects. It is designed as flat as possible. However, this is difficult since various types of equipment such as thrusters, control system, sensors, camera, and lights needed to be included in the UDR. In this paper, an architectural design of the UDR including all the equipment is presented. The architecture design of the disk-shaped UDR is shown in Fig. 2 and the UDR's specifications are described in table 1.

Fig. 1. The disk-shaped UDR

Table 1. Architecture of UDR system

Hull structure specifications	Diameter: 1.9m Height: 0.45m Weight: 80kg Max. Speed: 5 Knots
Propulsion module	3 vertical thrusters 3 horizontal thrusters
Control system module	Embedded computer: Cuwin 5200 Processors:DSP28335,XMEGA128A1
Navigation sensors	GPS: AsteRx1 IMU sensor: MTi DVL: NavQuest 600 USBL: Tracklink 1500 Pressure sensor: Sensys
Observation module	1 camera, 2 lights

The propulsion system is composed of three vertical and three horizontal thrusters. The vertical thrusters inside the vertical channels are mounted upward on the perimeter of the circular chassis. Using the vertical thrusters, the UDR can perform heaving, rolling and pitching motions. The horizontal thrusters are mounted on the perimeter of the circular chassis. They are installed in the side direction for horizontal motion. The horizontal thrusters are disposed 120 degrees apart facing outward. The disposition of the horizontal thrusters yields a vector propulsion force in the horizontal direction. And an RC motor using a coupled belt and pulley arrangement is installed on each horizontal thruster to rotate the thrusting direction by $\delta \in \left[-\frac{\pi}{12}, \frac{\pi}{12}\right]$ (rad). Using the horizontal thrusters, the UDR can perform surging, swaying, and yawing motions. Hence, 6 DOF motion is possible and will be presented in the following section.

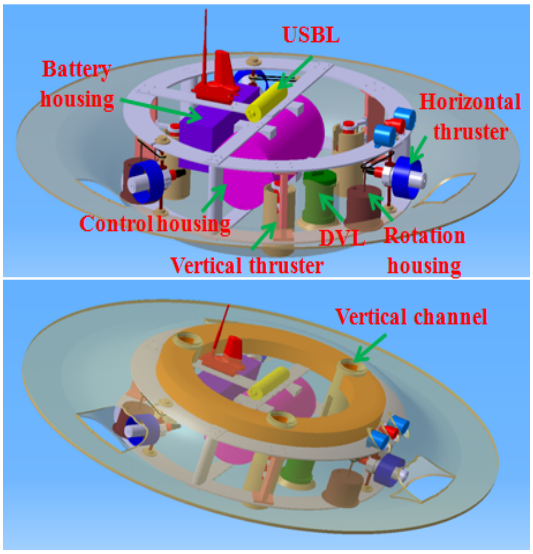

Fig. 2. The interior design of the UDR

2.2 Design of the Control System

As shown in Fig. 3, the UDR control system is composed of six parts which include the control system, navigation, power, propulsion, observation, and communication modules.

The power module is composed of a lithium battery pack and DC/DC converter board contained in the battery housing. This battery pack includes six 500W, 48V batteries parallel-connected to supply 3000W power to the UDR. The DC/DC converter module is used to lower the voltage for the sensor, light, and control subsystems.

The communication module is composed of a 24XStream RF module in the control housing. It transfers a standard asynchronous serial data stream over-the-air between devices at 2.4 GHz operating frequency up to 10 miles with a high gain antenna.

The observation module mainly contains one PHCS-C500 CCTV waterproof camera and two lights mounted on the UDR's fore. It records what is happening around the vehicle.

The propulsion control module shown in Fig. 3 is composed of three vertical 400HFS-L thrusters of 400W and three horizontal thrusters of 300W. The input power of the thrusters is fed using pulse width modulation (PWM) method. The thrusters are controlled by a RS-485 control signal according to a pre-defined protocol.

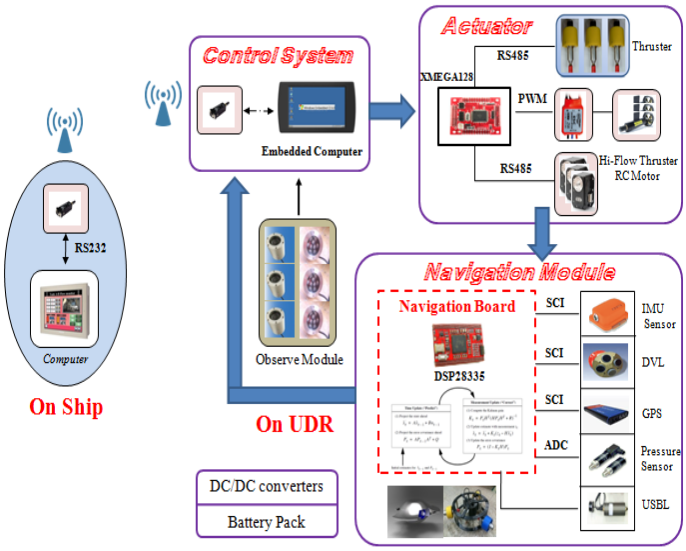

Fig. 3. Hardware architecture of UDR motion control system

The navigation module is composed of IMU, DVL, GPS, USBL and a pressure sensor. They are used to determine the position, velocity, acceleration, path, and distance traveled of the vehicle. The UDR is equipped with an inertial navigation system (INS), which calculates the position, velocity, and attitude of the vehicles from the data given by the IMU sensor. Since INS accumulates errors due to the inherent drift of dead-reckoning velocities and integration of acceleration, an Extended Kaman Filter (EKF) algorithm is implemented, which utilizes a wide range of navigation sensors, to compensate for the accumulation in position error [7].

The control system module contains the embedded computer Cuwin 5200 connected with two microprocessors TMS320F28335 (digital signal processors, DSP) and XMEGA128A1, which work together to perform all control tasks, as shown in Fig. 3.

3 Dynamic Modeling of the Vehicle

A coordinate system fixed at the body of the vehicle, called a body-fixed coordinate system, with its origin at the center of vehicle buoyancy, is used to build a dynamics model of the UDR. The motion of the body-fixed frame is described relative to an inertial or earth-fixed reference frame, as shown in Fig. 4.

In order to simplify the dynamics of the UDR model, the following assumptions are made:

- The vehicle is a rigid body of constant mass during operation.
- The effects of the vehicle's own wake are ignored.
- The vehicle is deeply submerged in a homogeneous fluid.

3.1 Vehicle Kinematics

As shown in Fig. 4, (x, y, z) and (ϕ, θ, ψ) are the position and orientation of the vehicle with respect to the inertial reference frame, respectively. The following coordinate transform relates the translational velocities between the body-fixed and inertial coordinates :

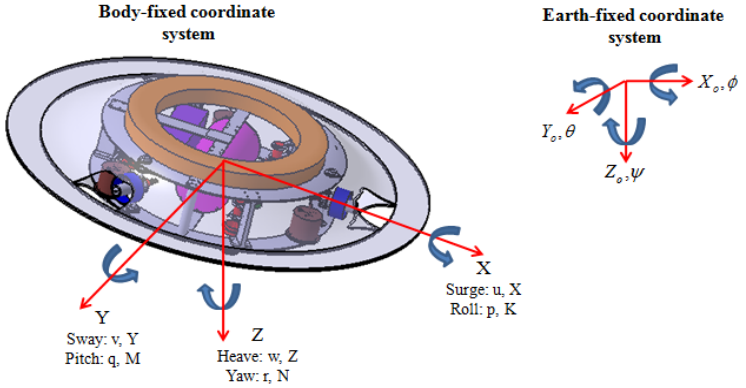

Fig. 4. Body-fixed and inertial coordinate systems

$$\begin{bmatrix} \dot{x} \\ \dot{y} \\ \dot{z} \end{bmatrix} = J_1(\eta_2) \begin{bmatrix} u \\ v \\ w \end{bmatrix}. \tag{1}$$

where

$$J_1(\eta_2) = \begin{bmatrix} c\psi c\theta & -s\psi c\phi + c\psi s\theta s\phi & s\psi s\phi + c\psi s\theta c\phi \\ s\psi c\theta & c\psi c\phi + s\psi s\theta s\phi & -c\psi s\phi + s\psi s\theta c\phi \\ -s\theta & c\theta s\phi & c\theta c\phi \end{bmatrix}.$$

The second coordinate transform relates the rotational velocities between the body-fixed and inertial coordinates:

$$\begin{bmatrix} \dot{\phi} \\ \dot{\theta} \\ \dot{\psi} \end{bmatrix} = J_2(\eta_2) \begin{bmatrix} p \\ q \\ r \end{bmatrix}. \tag{2}$$

where

$$J_2(\eta_2) = \begin{bmatrix} 1 & s\phi t\theta & c\phi t\theta \\ 0 & c\phi & -s\phi \\ 0 & s\phi / c\theta & c\phi / c\theta \end{bmatrix}.$$

Note that $J_2(\eta_2)$ is not defined for pitch angle $\theta = \pm 90^0$ as the vehicle motion does not ordinarily approach this singularity. If it becomes necessary to model the vehicle motion through extreme pitch angles, an alternate kinematic representation such as quaternions or Rodriguez parameters can be used.

3.2 Vehicle Dynamics

The In the following sections, the 6 DOF nonlinear dynamic equations of motion are conveniently expressed as:

$$M\dot{\upsilon} + C(\upsilon)\upsilon + D(\upsilon)\upsilon + g(\eta) = \tau. \tag{3}$$

where

M: Inertia matrix (including added mass)

$C(\upsilon)$: Matrix of Coriolis and centripetal terms (including added mass)

$D(\upsilon)$: Damping matrix

$g(\eta)$: Vectors of gravitational forces and moments

τ: Vectors of control inputs

Given that the origin of the body-fixed coordinate system is located at the center of buoyancy as noted, from equation (3), the 6-DOF equations of motion for a rigid body can be expressed in terms of body-fixed coordinates [8]:

$$
\begin{aligned}
&m[\dot{u}-vr+wq-x_g(q^2+r^2)+y_g(pq-\dot{r})+z_g(pr+\dot{q})]=\sum X\\
&m[\dot{v}-wp+ur-y_g(r^2+p^2)+z_g(pr-\dot{p})+x_g(qp+\dot{r})]=\sum Y\\
&m[\dot{w}-uq+vp-z_g(p^2+q^2)+x_g(rp-\dot{q})+y_g(rq+\dot{p})]=\sum Z\\
&I_{xx}\dot{p}+(I_{zz}-I_{yy})qr-(\dot{r}+pq)I_{xz}+(r^2-q^2)I_{yz}+(pr-\dot{q})I_{xy}\\
&\quad+m[y_g(\dot{w}-uq+vp)-z_g(\dot{v}-wp+ur)]=\sum K\\
&I_{yy}\dot{q}+(I_{xx}-I_{zz})rp-(\dot{p}+qr)I_{xy}+(p^2-r^2)I_{xz}+(qp-\dot{r})I_{yz}\\
&\quad+m[z_g(\dot{u}-vr+wq)-x_g(\dot{w}-uq+vp)]=\sum M\\
&I_{zz}\dot{r}+(I_{yy}-I_{xx})pq-(\dot{q}+rp)I_{yz}+(q^2-p^2)I_{xy}+(rq-\dot{p})I_{xz}\\
&\quad+m[x_g(\dot{v}-wp+ur)-y_g(\dot{u}-vr+wq)]=\sum N
\end{aligned}
\tag{4}
$$

where

- u, v, w: Surge, sway, heave velocities respectively.
- p, q, r: Roll, pitch, yaw rates.
- X, Y, Z: External forces.
- K, M, N: External moments.
- x_g, y_g, z_g : Center of gravity with respect to the origin at the center of buoyancy.
- I_{ab} : Moments of inertia with respect to the origin at center of buoyancy (a, b symbolize x, y, z).

3.3 Mechanics of the Propulsion System

With the 120-degree symmetrical vector disposition of the horizontal and vertical thrusters, the UDR has 6 DOF and can carry out robust underwater motion under side disturbances. We analysed the propulsion system for two cases: horizontal propulsion and vertical propulsion.

1) Horizontal propulsion module

Each horizontal thruster can also rotate about their individual mounting point using a coupled belt and pulley arrangement within the bound $\delta \in \left[-\frac{\pi}{12}, \frac{\pi}{12}\right]$ (rad).

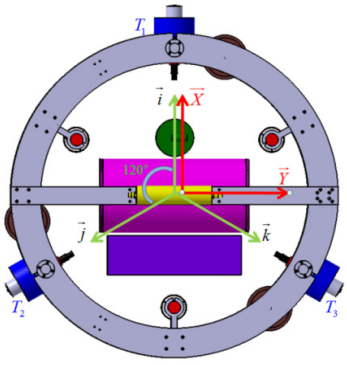

Fig. 5. Horizontal thrust forces with $\delta = 0$ (rad)

a) In case $\delta = 0$ (rad) shown in Fig. 5, the total force $\overrightarrow{F_T}$ from the three thrust forces $\overrightarrow{F_{T1}}, \overrightarrow{F_{T2}}, \overrightarrow{F_{T3}}$ on the plane XOY of the body-fixed coordinates O-XYZ can be expressed as:

$$\overrightarrow{F_T} = \overrightarrow{F_{T1}} + \overrightarrow{F_{T2}} + \overrightarrow{F_{T3}}. \tag{5}$$

$$X_T.\vec{X} + Y_T.\vec{Y} = F_{T1}.\vec{i} + F_{T2}.\vec{j} + F_{T3}.\vec{k} \tag{6}$$

$$\begin{aligned} X_T.\vec{X} + Y_T.\vec{Y} &= (F_{T1}.\sin\alpha + F_{T2}.\sin\beta + F_{T3}.\sin\theta)\vec{X} \\ &+ (F_{T1}.\cos\alpha + F_{T2}.\cos\beta + F_{T3}.\cos\theta)\vec{Y} \end{aligned} . \tag{7}$$

The total thrust forces along the X-axis and Y-axis, respectively:

$$\begin{bmatrix} X_T \\ Y_T \end{bmatrix} = \begin{bmatrix} \sin\alpha & \sin\beta & \sin\theta \\ \cos\alpha & \cos\beta & \cos\theta \end{bmatrix} \begin{bmatrix} F_{T1} \\ F_{T2} \\ F_{T3} \end{bmatrix}. \tag{8}$$

Rewriting this yields

$$\begin{bmatrix} X_T \\ Y_T \end{bmatrix} = \begin{bmatrix} 1 & -0.5 & -0.5 \\ 0 & -\frac{\sqrt{3}}{2} & \frac{\sqrt{3}}{2} \end{bmatrix} \begin{bmatrix} F_{T1} \\ F_{T2} \\ F_{T3} \end{bmatrix}. \tag{9}$$

where $\vec{i}, \vec{j}, \vec{k}$ are the unit vectors of the thrusters $\overrightarrow{F_{T1}}, \overrightarrow{F_{T2}}, \overrightarrow{F_{T3}}$, $\alpha = \frac{\pi}{2}$ is the angle of $\overrightarrow{OY}$ with $\vec{i}$, $\beta = \frac{7\pi}{6}$ is the angle of $\overrightarrow{OY}$ with $\vec{j}$ and $\theta = \frac{11\pi}{6}$ is the angle of $\overrightarrow{OY}$ with $\vec{k}$. Through Eq. (9), the maximum resultant force X_T is 2 F_{T1} along the X axis and the maximum resultant force Y_T is along the Y axis $\sqrt{3}F_{T1}$ when $F_{T1} = F_{T2} = F_{T3}$.

b) In case $\delta \neq 0$ (rad) described in Fig. 6, the thrust forces include the force along the UDR center $\overrightarrow{F_{TnP}}$ and the force $\overrightarrow{F_{TnR}}$ perpendicular to $\overrightarrow{F_{TnP}}$ for n=1, 2, 3. We have:

$$\overrightarrow{F_{T1}} = \overrightarrow{F_{T1P}} + \overrightarrow{F_{T1R}}. \tag{10a}$$

$$\overrightarrow{F_{T2}} = \overrightarrow{F_{T2P}} + \overrightarrow{F_{T2R}}. \tag{10b}$$

$$\overrightarrow{F_{T3}} = \overrightarrow{F_{T3P}} + \overrightarrow{F_{T3R}} . \tag{10c}$$

$$F_{Tn} = \left|\overrightarrow{F_{T1}}\right| = \left|\overrightarrow{F_{T2}}\right| = \left|\overrightarrow{F_{T3}}\right| . \tag{11}$$

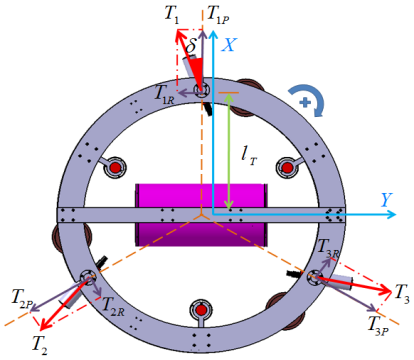

Fig. 6. Horizontal thrust forces with $\delta \neq 0$ (rad)

The total force $\overrightarrow{F_T}$ in this case is zero:

$$\overrightarrow{F_T} = \overrightarrow{F_{T1}} + \overrightarrow{F_{T2}} + \overrightarrow{F_{T3}} = \vec{0} \tag{12}$$

The moment N_T makes UDR rotate about the Z-axis:

$$N_T = 3F_{Tn} l_T \sin\delta \tag{13}$$

where L_T is the distance from the center to the thruster side.

2) The vertical propulsion module

A vertical thruster is placed at a distance l_H from the center of the vehicle. It produces the vertical forces in the UDR Z-axis direction, as shown in Fig. 7.

The total vertical force in the Z-axis direction:

$$Z_H = F_{H1} + F_{H2} + F_{H3} \tag{14}$$

The moment about the X-axis:

$$K_H = \frac{\sqrt{3}}{2} l_H (-F_{H2} + F_{H3}) \tag{15}$$

The moment about the Y-axis:

$$M_H = l_H (\frac{F_{H2} + F_{H3}}{2} - F_{H1}) \tag{16}$$

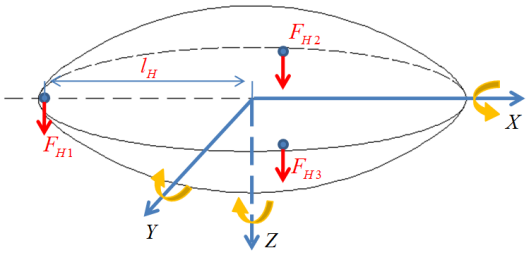

Fig. 7. The vertical forces on the UDR

In the equations of motion, the external forces and moments include hydrostatic forces and moments, hydrodynamic damping, added mass, body lift, and the propeller thrust and torque detailed in previous sections. According to the previous dynamic equation (4) and the propulsion mechanics equations (9), (12), (13), (14), (15), (16), the external forces and moments can be rewritten as follows:

$$\begin{aligned}
&\sum X = X_{HS} + X_{u|u|}u|u| + X_{\dot{u}}\dot{u} + X_{wq}wq + X_{qq}qq + X_{vr}vr \\
&+X_{rr}rr + X_T \\
&\sum Y = Y_{HS} + Y_{v|v|}v|v| + Y_{r|r|}r|r| + Y_{\dot{v}}\dot{v} + Y_{\dot{r}}\dot{r} + Y_{ur}ur + Y_{wp}wp \\
&+Y_{pq}pq + Y_{uv}uv + Y_T \\
&\sum Z = Z_{HS} + Z_{w|w|}w|w| + Z_{q|q|}q|q| + Z_{\dot{w}}\dot{w} + Z_{\dot{q}}\dot{q} + Z_{uq}uq \\
&+Z_{vp}vp + Z_{rp}rp + Z_{uw}uw + Z_H \\
&\sum K = K_{HS} + K_{p|p|}p|p| + K_{\dot{p}}\dot{p} + K_H \\
&\sum M = M_{HS} + M_{w|w|}w|w| + M_{q|q|}q|q| + M_{\dot{w}}\dot{w} + M_{\dot{q}}\dot{q} + M_{uq}uq \\
&+M_{vp}vp + M_{rp}rp + M_{uw}uw + M_H \\
&\sum N = N_{HS} + N_{v|v|}v|v| + N_{r|r|}r|r| + N_{\dot{v}}\dot{v} + N_{\dot{r}}\dot{r} + N_{ur}ur + N_{wp}wp \\
&+N_{pq}pq + N_{uv}uv + N_T
\end{aligned} \tag{17}$$

4 Motion Analysis of the UDR

A VPMM (Vertical Planar Motion Mechanism) test was carried out to find the hydrodynamic coefficients of the UDR for its control. That is, the VPMM test was carried out with the aim of measuring the hydrodynamic forces on the vehicle when changing the motion of the vehicle; e.g. Change of angle of attack, velocity, acceleration etc. The hydrodynamic forces for the VPMM test were obtained for the pure heave motion and the pure pitch motion of the vehicle.

For the case of pure heave motion, the vehicle moves in a sinusoidal fashion with amplitude (z_0), but no pitch angle (θ_0) as shown in Fig. 8 (A). Pure pitch motion, on the other hand, is such that the vehicle moves in a sinusoidal fashion, but this time with a pitch angle (θ_0) at the center of gravity of the vehicle body and the longitudinal body axis is oriented tangential to the path, as shown in Fig. 8 (B).

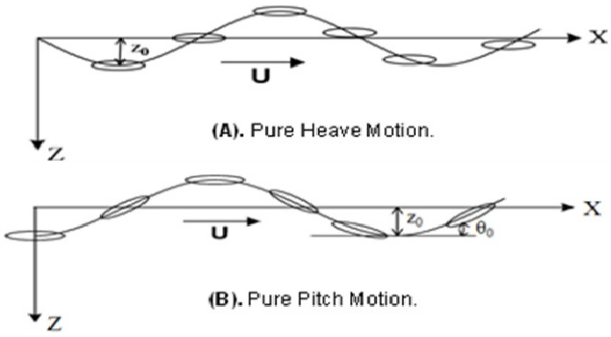

Fig. 8. Description of Pure Heave Motion (A) and Pure Pitch Motion (B)

Conventionally, the tests for the prediction of drag, and motion of an underwater robot are carried out in a large model basin equipped with a towing carriage, and dynamometer, making the test process expensive. The development of commercial codes for CFD analysis now make it possible to predict drag and propulsion performance of a ship or submersible vehicles such as an underwater robot without using a physical model test basin [9].

The position of the body should be defined and specified for motion analysis, which is the VPMM simulation. The motion of the UDR body is defined as shown in Fig. 9 (top) by using the ANSYS-CFX Command Language (CCL) to simulate the pure heave motion or pure pitch motion.

'Tetrahedral' and 'Prism' elements were employed for generating nodes and elements in the fluid domain. A hybrid mesh is created by merging the two mesh structures, and embodied for the CFD analysis by the "ANSYS-CFX-MESH" mesh generator as shown in Fig. 9 (bottom). The mesh properties for the UDR motion study are shown in table 2.

Table 2. Density of the model employed for the UDR motion analysis

Total no. of Nodes	523,899
No. of Faces	57,180
Total no. of elements	1,457,504
No. of Tetrahedrals	646,944
No. of Prisms (for B.C.)	810,560

The x-directional velocity of the vehicle is 1 m/s, and the pure heave motion was carried out with the period (Tt) of 8 seconds while the pure pitch motion has the period (Tt) of 12 seconds. Total computation time (T) is 24 seconds and time step (Δt) is 0.1 second for the CFD moving analysis.

The x-directional velocity of the vehicle is 1 m/s, but the boundary layer grows along the mid-body and the flow is accelerated as it reaches the stern so the velocity of the flow is higher than the x-directional velocity of the vehicle (1.917 m/s - Pure heave motion; 1.186 m/s - Pure pitch motion).

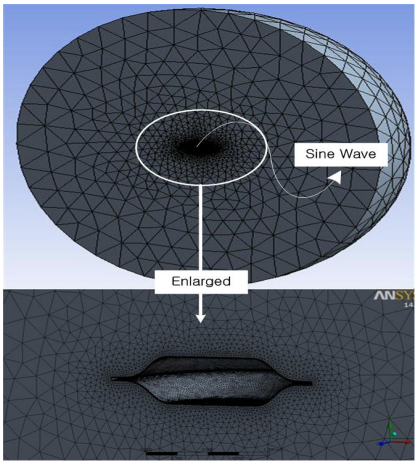

Fig. 9. General view of the mesh (top) and the hybrid mesh generated adjacent to the main body (bottom) of the UDR)

The x and z-axis directional forces of the pure heave motion and pure pitch motion obtained by the CFD analysis are shown in Fig. 10. The added mass and inertia of the vehicle are derived from these hydrodynamic forces .

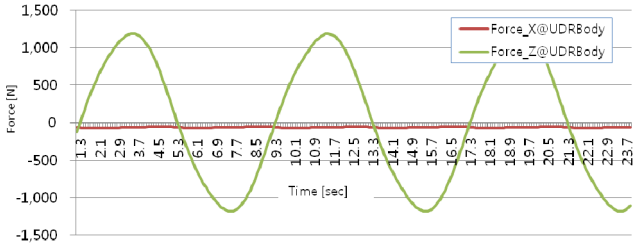

(a) Pure Heave Motion (T_t=8 [sec])

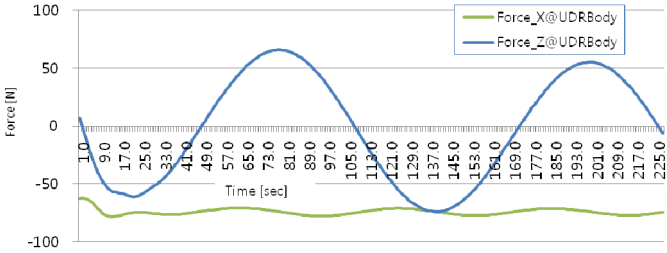

(b) Pure Pitch Motion (T_t=12 [sec])

Fig. 10. X and Z-directional forces on the UDR Body

5 Conclusion

An analysis on the architecture and control system of a new 6 DOF disk-shaped underwater disk robot (UDR) was presented. The streamline disk shape is chosen for the hull to allow the UDR to move flexibly with a low drag force in the horizontal direction.

The dynamics analysis of the UDR including that of the actuator mechanics were presented. And the heave and pitch motion simulation studies of the UDR were carried out with the computational fluid dynamics (CFD) software. We can use these results to estimate the hydrodynamic coefficients of the UDR for its control.

References

1. Manley, J.E.: Unmanned Surface Vehicles, 15 Years of Development. In: Proceedings of Oceans 2008, Quebec City, Canada (September 2008)
2. Wernli, R.L.: AUV'S - The Maturity of the Technology. In: Proceedings of Oceans 1999. MTS/IEEE, Seattle (1999)
3. Roman, C., Pizarro, O., Eustice, R., Singh, H.: A New Autonomous Underwater Vehicle for Imaging Research. In: Proceedings of Oceans 2000. MTS/IEEE, Providence (2000)
4. Gomes, R.M.F., Sousa, A., Fraga, S.L., et al.: A New ROV Design: Issues on Low Drag and Mechanical Symmetry. In: Proceedings of Oceans, Europe (June 2005)
5. Wang, T., Ye, X., Wang, L., Zhang, C.: Hydrodynamic Analysis and Optimization for Dish Shaped Underwater Robot. In: Proceedings of the 2011 IEEE International Conference on Mechatronics and Automation, Beijing, China, August 7-10 (2011)
6. Dudek, G., Giguere, P., Prahacs, C., et al.: AQUA: An Amphibious Autonomous Robot. Proceedings of the Computer Journal 40(1) (January 2007)
7. Titterton, D.H., Weston, J.L.: Strapdown Inertial Navigation Technology, 2nd edn. Americn Institute of Aeronautics and Astronautics (2004)
8. Fossen, T.I.: Guidance and Control of Ocean Vehicles. John Wiley & Son, New York (1994)
9. Joung, T.H., Sammut, K., He, F., Lee, S.K.: Shape Optimization of an Autonomous Underwater Vehicle with a Ducted Propeller using Computational Fluid Dynamics Analysis. International Journal of Naval Architecture & Ocean Engineering 4, 44–56 (2012)